Molecular Crystals and Liquid Crystals

ISSN: 1542-1406 (Print) 1563-5287 (Online) Journal homepage: http://www.tandfonline.com/loi/gmcl20

Domain Patterns in Homogeneous and Random Perturbed Nematic Liquid Crystals: A Simulation Study

Amid Ranjkesh, Milan Ambrožič, T. J. Sluckin & Samo Kralj

To cite this article: Amid Ranjkesh, Milan Ambrožič, T. J. Sluckin & Samo Kralj (2015) Domain Patterns in Homogeneous and Random Perturbed Nematic Liquid Crystals: A Simulation Study, Molecular Crystals and Liquid Crystals, 615:1, 26-41, DOI: 10.1080/15421406.2015.1068467

To link to this article: http://dx.doi.org/10.1080/15421406.2015.1068467

Mol. Cryst. Liq. Cryst., Vol. 615: pp. 26–41, 2015

ISSN: 1542-1406 print/1563-5287 online
DOI: 10.1080/15421406.2015.1068467

Taylor & Francis
Taylor & Francis Group

Domain Patterns in Homogeneous and Random Perturbed Nematic Liquid Crystals: A Simulation Study

AMID RANJKESH,[1,*] MILAN AMBROŽIČ,[1,2]
T. J. SLUCKIN,[1,3] AND SAMO KRALJ[1,2]

[1]Faculty of Natural Sciences and Mathematics, University of Maribor, Maribor, Slovenia
[2]Condensed Matter Physics Department, Jožef Stefan Institute, Ljubljana, Slovenia
[3]Division of Mathematical Sciences, University of Southampton, Southampton, United Kingdom

We have simulated lattice models of homogenous and randomly perturbed systems exhibiting continuous symmetry breaking, concentrating on domain sizes and configuration character. The system consists of rod-like objects within a cubic lattice interacting via a Lebwohl–Lasher-type interaction at temperature T*, but including impurities at concentration* p *imposing a random anisotropy field-type disorder, coupled with anchoring strength* W *to neighboring host director molecules. An example of such systems represents nematic LC or nanotubes. We study molecular domain patterns as a function of* p*,* W*,* T*, and sample history. Histories are defined either by a temperature-quenched history (*TQH*), a field-quenched history (*FQH*) or from an annealed history (*AH*). Finite size-scaling is used to determine the nature of the orientational ordering correlations. We distinguish three different kinds of phase. Short ranged order (*SRO*) implies exponential decay of orientational correlations. Quasi-long-range order (*QLRO*) sustains algebraic decay of orientational correlations. True long-range order (*LRO*) implies a non-zero order parameter in the thermodynamic limit in the absence of an external field. In the* TQH *case for particular values of p and* W*, we find* SRO *or* QLRO*, with possible LRO at very low* W *and* p*. For* FQH*, in the limit of very low* W *and* p*, we observe* LRO*, which gives way to an SRO regime with increasing* p *and* W*. Comparing* FQH *and* TQH *histories at particular values of* T*, we saw* QLRO *and* SRO *respectively. The crossover between regimes depends on history, but in general, the* FQH *yields a more ordered phase than the* AH*, which in turn yields a more ordered phase than the* TQH*. In phases in which* SRO *occurs, the orientational correlation length in the weak-disorder limit obeys universal Imry-Ma scaling* $\xi_d \sim W^{-2/(4-d)}$.

Keywords Lebwohl-Lasher model; Nematic liquid crystals; disorder; orientational order; Imry-Ma theorem; Finite analysis

*Address correspondence to Amid Ranjkesh, Faculty of Natural Sciences and Mathematics, University of Maribor, Koroška 160, 2000, Maribor, Slovenia. Email: amidranjkesh@gmail.com

1. Introduction

Liquid crystals (LCs) are materials can exhibit transitions between multiple phases. LCs exhibit a rich different structures and phases that can display almost all physical phenomena. Two commonly studied LC phases are the isotropic and nematic phases. The isotropic phase exhibits no translational or orientational order, while the nematic phase exhibits short-range orientational order. The structure, thermodynamics, and phase behavior of liquid crystals in disordered porous media has attracted much attention over the past decade [1–10].

In particular, the isotropic-nematic transition has been experimentally characterized, mainly by means of optical, calorimetric and magnetic resonance techniques. The structure of liquid crystals is optically anisotropic and their structures are visible; they are easily controlled by the confining surfaces and applying an external electric or magnetic field.

The nature of the isotropic–nematic (*I-N*) phase transition is relevant for many technological applications. Liquid crystals consisting of anisotropic molecules, in randomly connected networks of pores [6], have attracted increasing interest lately because of their importance in technological applications and nanotechnology.

A characteristic feature of a nanoparticle is that at least one of its dimensions is of the order of nanometers. Such systems expected to play an important role in the emerging field of nanotechnology and in composites with extraordinary material properties. These mixtures can generally exhibit behaviors which are not encountered in either of isolated components, opening the possibility of new applications. In addition, there has been strong interest in the phase and structural behavior of randomly perturbed liquid crystals (LCs)[6].

The simplest liquid crystalline state is a nematic phase in which the molecules exhibit only orientational long-range order and no translational long-range order. Here there is a bulk broken symmetry. However, liquid crystals confined to porous media are thought to behave as though there is a spatially random perturbation [6]. This picture is supported by a number of experimental studies involving light [8] and X-ray scattering [9]. Disorder has been typically introduced by confining soft materials to different porous matrices like aeroglas, Vycor glass or mixed LCs with nanoparticles or colloids [11–17].

The isotropic (with neither orientational nor translational long-range order) to nematic (I-N) transition [18–25] of thermotropic liquid crystals embedded in porous networks has been characterized using various experimental techniques [14]. Many experimental techniques have been used various types of NMR studies [18], magnetically-induced birefringence [18], static and dynamic light scattering [14, 23], various types of calorimetry [14, 16, 25] and dielectric spectroscopy [16].

The background to the pattern dynamics is as follows. When LCs are suddenly quenched from the isotropic to the lower symmetry nematic phase, then unavoidably a domain pattern forms [8]. The domain pattern dynamics in a pure bulk system are described by the Kibble-Zurek mechanism [10, 17], which was originally introduced to explain the formation of topological defects in the early universe following the big bang [10]. The domain sizes increase in size as a function of time [7, 28]. In pure system, this growth continues indefinitely, but in glassy systems, the domains can saturate in size, as a result of liquid crystal defect pinning [29-31]. However, the domain positions are not in general fixed, and the domain size saturation is a signature of a low temperature glassy phase. Studies so far have mainly focused on structural and phase behavior [17–31]. Further signatures of glassy states can also involve memory effects, slow dynamics and the existence of a difference on the response to external fields between field-cooled and zero-field-cooled systems [23, 32].

However, detailed theoretical predictions and experimental studies are not well matched especially for relatively weak disorder. In particular, random field models appear to predict the possibility of phases with short range and quasi-long range order, and there is some controversy over the fate of a truly long range order phase in the presence of disorder.

Two model glassy systems which have been studied in the literature are the random anisotropy nematics (*RAN*)[10] and the Sprinkled Silica Spin (*SSS*) [8] models. Both pictures are based on the Lebwohl-Lasher lattice model [33]. In the *RAN* model, each local spin is coupled to an uncorrelated random anisotropy field. In the SSS model, on the other hand, some of the spins are regarded as impurities, and are frozen in random directions [23]. These frozen spins are randomly distributed spatially, and might be thought of as representing the silica branches in a porous medium.

The low temperature phases of these model glassy systems seem to exhibit interesting pattern dynamics, which have however, only been incompletely explored. We note that the presence of local fields implies that even in the high temperature phase, there is some local order, in contrast to the case in which there is no externally imposed order at all. When the external field is uniform, we refer to the high temperature phase as a paranematic phase, and simple theories of the RAN model draw much intuition from this case [10].

In fact the liquid crystal polymer models [10, 34] are just examples of a whole family of random field spin models, with applications in particular in magnetism. One paradigm for such studies is that due to Imry and Ma [34]. In anisotropy random magnets (the paradigm for the RAN liquid crystal model), Imry and Ma showed that even infinitesimally weak random perturbations destroy equilibrium long-range order. They predict the scaling behavior $\xi_d \propto W^{\frac{-2}{(4-d)}}$ for weak enough disorder strength; where ξ_d is the characteristic domain size and W a measure of the strength of the disorder. The idea is that if the domains are too small, the system keeps a large number of boundaries, whose energy is unfavorable. However, if they are too large, they cannot order locally to take improvement of the local random fields. The balance is a universal domain pattern, characterized by exponential correlations on a supra-molecular scale. The literature labels such order as short range (or "short-range order", *SRO*), because of the exponential form of the correlations, contrasting it with algebraically decaying orientational correlations ("quasi-long-range order" *QLRO*), and true long-range order (*LRO*). Although the validity of the Imry-Ma theorem, which shows that the long-range order is unstable with respect to a domain pattern, is not in doubt, there has been much debate as to what are the equilibrium low temperature phases, whether and when QLRO prevails against the Imry-Ma SRO phase, and what conditions are required for Imry-Ma SRO to be observed (see e.g. [5,19]).

In this report we analyze a model, to be described in more detail below, intermediate between the RAN and the SSS models, using a Brownian simulation method. The model includes a parameter describing the impurity-liquid crystal anchoring strength, as well as the impurity concentration p. The nature of the low temperature phase is difficult to establish unambiguously. For this reason finite size scaling methods are also used to provide extra evidence as to whether a phase is SRO, QLRO or LRO. Our focus here is on the manner in which the sample history affects the phase behavior of a low temperature nematic structure. The plan of the paper is as follows. In Sec. II we present our model. The simulation results are presented and discussed in Sec. III. In the last section, we summarize our results.

II. Model

We use a semi-microscopic lattice model consisting of rod-like LC molecules and rod-like impurities. The orientational ordering of either of them at an *ith* lattice site is presented by

a unit vector $\vec{S}_i$ exhibiting head-to-tail invariance (i.e., states $\vec{S}_i$ and -$\vec{S}_i$ are equivalent). The LC molecules ($\vec{S}_i = \vec{s}_i$) and impurities ($\vec{S}_i = \vec{m}_i$) are henceforth referred to as LC spins and impurity spins, respectively. They occupy N^3 lattice sites of a 3D cubic simulation cell. A typical value of $N = 70$ is chosen. An *i-th* site is occupied either by a LC or an impurity spin. Impurities of concentration p are randomly distributed in space, and their orientations are frozen and randomly distributed in direction. Note that the system possesses pN^3 impurities.

The total interaction of the system is given as the sum over the lattice site contributions $F = \sum_i f_i$, where [8, 10, 17]

$$f_i = -\frac{1}{2}\sum_j J_{ij}(\vec{S}_i \cdot \vec{S}_j)^2 - B^2(\vec{s}_i \cdot \vec{e}_B)^2. \tag{1}$$

The first part of the free energy functional includes the spin interactions between the 6 nearest neighbors. For convenience, the factor 1/2 is added in order to avoid double-counting.

Here, J is the coupling constant that describes the ordering interaction among neighboring molecules tending to orient directors parallel or antiparallel. The coupling constant can have one of the three values: 1) 0, if both neighbors are impurities 2) $J_{ij} = J > 0$, if both neighbors are LC spins; and 3) $J_{ij} = W > 0$ for neighboring LC and impurity spins. The second part of Eq. (1) defines the interaction between the external field $\vec{B} = B\vec{e}_b$ and the LC spins, where $|\vec{e}_b| = 1$. For this article we set $B = 0$ for our simulations.

We defined ordering in the three dimensional ($d = 3$) Cartesian coordinate frame (x, y, z), whose axes point along unit vectors e_x, e_y and e_z, respectively. In simulations we take into account the normalization $|\vec{S}_i| = 1$ by introducing the Lagrange multipliers λ_i in the functional $F* = \sum_i f_i*$, where

$$f_i* = \lambda_i(\vec{S}_i.\vec{S}_i - 1) + f_i \tag{2}$$

The functional F^* is minimized with respect to LC spins $\vec{s}_i$, yielding $(1-\mathrm{p})N^3$ equations:

$$\vec{R}_i = \frac{1}{2}\frac{\partial F^*}{\partial \vec{s}_i} \equiv \sum_j J_{ij}\vec{g}(\vec{S}_i, \vec{S}_j) + B^2\vec{g}(\vec{S}_i, \vec{e}_B) = 0 \tag{3}$$

Here $\vec{R}_i$ is commonly referred to as the residuum and $\vec{g}(\vec{v}_1, \vec{v}_2)$ is defined as

$$\vec{g}(\vec{v}_1, \vec{v}_2) = (\vec{v}_1 \cdot \vec{v}_2)[(\vec{v}_1 \cdot \vec{v}_2)\vec{v}_1 - \vec{v}_2] \tag{4}$$

For finite temperatures, the final states reached via the "real-time" relaxation process. The change of spin components in a time step Δt is given by

$$\vec{s}_i(t + \Delta t) = \vec{s}_i(t) - \frac{D\Delta t}{k_B T}\frac{\partial F^*}{\partial \vec{s}_i}(t) + \Delta\vec{S}_T \tag{5}$$

Here D is the appropriate degenerate rotation diffusion constant of the system and k_B is the Boltzmann constant. The second term on the right hand side of Eq. (5) corresponds to the mechanical torque which tends to rotate a LC spin towards equilibrium, while the third term $\Delta\vec{S}_T$ represents the random thermal fluctuations.

We henceforth set $J = 1$ and introduce a dimensionless time step $\Delta t^* = D\Delta t$ and temperature $T^* = kBT/J$. In the simulations it is set $\Delta t^* \approx 0.016$ in order to obtain sensible reference results in bulk nematic phase.

It follows

$$\vec{s}_i(t + \Delta t) = \vec{s}_i(t) - 2\frac{\Delta t*}{T*}\vec{R}_i(t) + \Delta\bar{S}_T \tag{6}$$

Using this method the fixed point configurations are calculated, for which the macroscopic properties of the system do not anymore change as a function of time. Therefore, these configurations correspond either to equilibrium or to metastable states surrounded by relatively high-energy barriers.

The configurations the average tensor order parameter $\underline{Q}$ of a system and the orientational correlation function *G(r)* have been calculated. The traceless symmetric order parameter tensor, describing the average behavior of the whole system, is defined as

$$\underline{Q} = \frac{1}{2}\left(3\left\langle\vec{s}_i \otimes \vec{s}_i\right\rangle - \underline{I}\right). \tag{7}$$

The brackets $< \ldots >$ denote a spatial averaging, $\underline{I}$ is the identity matrix and $\otimes$ stands for the tensor product. The average scalar order parameter of the system S is defined as the largest eigenvector of $\underline{Q}$.The correlation function is calculated as

$$G(r) = \frac{1}{2}\left(3 < (\vec{s}_i \cdot \vec{s}_j)^2 > -1\right), \tag{8}$$

where $< \ldots >$ is the average over only those LC *spin* pairs which are separated by the distance r.

For SRO or QLRO phase behavior, $G(r \to \infty) \to 0$. However for LRO, $G(r \to \infty) \to g_\infty \sim S^2$. In general, one expects an exponential decay towards a saturated value of *G(r)* on increasing r for both LRO and SRO. On the other hand, for QLRO, there is algebraic decay of correlations, and thus, by definition [21],$G(r) \propto r^{-\alpha}$.

In order to obtain structural details from *G(r)* for a finite system the correlation function is fitted using the empirical ansatz

$$G^{(0)}(r) = a_0 e^{-kr} + b_0, \tag{9}$$

or

$$G^{(1)}(r) = \frac{a_1 e^{-k_1 r}}{r} + b_1, \tag{10}$$

where a_0, a_1, b_0, b_1, k and k_1 are adjustable parameters. Note that, roughly speaking $b_0 \sim b_2 \sim S^2$, and $\xi = 1/k$ estimates an average linear size of a relatively well-correlated region, referred to as a domain. The ansatz $G^{(1)}(r)$ is suitable for structures exhibiting either LRO or SRO.

The parameter $b_0 \sim b_2 \sim S^2$ measure the LC ordering on large scale: $S = 0$ indicates *SRO* while $S > 0$ indicates LRO or QLRO. On the other hand, the expression $G^{(2)}(r)$ is more appropriate for studying structures possessing QLRO:

$$G^{(2)}(r) = \frac{a_2}{r^\alpha} + b_2 \tag{11}$$

and a_2, b_2 and α are adjustable parameters. One expects $G^{(2)}(r \to \infty) \to 0$. However, the decay of correlations with distance is relatively weak, and finite-size effects are thus expected to be important.

Estimates for the power law α could be determined using a finite size scaling analysis [35–37] of $S = S(L)$, using the relationship

$$S \propto L^{-\gamma} \tag{12}$$

For *SRO*, the mean order parameter in a system of N particles would be given by $S \sim 1/\sqrt{N} = L^{-\frac{3}{2}}$, implying $\gamma = \frac{3}{2}$ in this case. By contrast, in the case of *LRO*, the order parameter tends to a finite non-zero value for large system size L, and hence $\gamma = 0.0$. *QLRO* is indicated by intermediate values of, with $\gamma = \alpha/2$, so long as $\alpha \leq 3$, although if $\alpha \geq 3$, the *SRO* finite-size scaling result is recovered.

In simulations, the initial configuration was either a set of randomly distributed director orientations, or a sample, homogeneously aligned along a symmetry breaking direction. In the latter case, the directors are initially homogeneously aligned along e_x. We henceforth refer to these cases as the I) *TQH* (temperature-quenched history) and II) *FQH* (field-quenched history), respectively. The *TQH* case can be experimentally realized by quenching the system from the isotropic phase to the ordered phase without an external field (i.e. $B = 0$). This can be achieved either via a sudden decrease of temperature or sudden increase of pressure. The *FQH* case can be realized by applying first a strong homogeneous external field B along a symmetry breaking direction. After a sufficiently good alignment is achieved, the field is switched off. In order to reduce the influence of statistical variations, simulations were generally repeated $N_{rep} \sim 10$ times for a given set of parameters (i.e. W, p and a chosen initial condition). Our interest was to find the main structural characteristic of S_i patterns as a function of p, W and a history of such systems. Some further simulations were carried out by cooling the system slowly from high temperatures (i.e. annealing); this is the AH (annealed history).

III. Results and Discussion

The typical lattice size in our calculations was $N = 70$. We chose different values of anchoring strength, W, varied impurity concentration p and temperature T. We followed the evolution of the scalar order parameter S and the domain size ξ belonging to the correlation function eq. (8) according to the form of eq. (9a) respectively. Since both impurities and thermal fluctuations contribute to orientational disorder in the nematic phase, S is reduced on increasing either impurity concentration or temperature. Moreover, we tested the system behavior upon increasing temperature according to different scenarios relating to initial system configurations: *FQH*, *TQH* and *AH* initial orientation of nematic spins.

In *TQH* is disorder orientation followed by spin relaxation, but for each higher temperature, the numerical procedure takes the last (relaxed) spin configuration of the previous (a little lower) temperature before relaxation at this temperature begins. (this is not temperature quenching; temperature quenching consists of starting with a random configuration and then imposing a finite temperature T! Is this what you mean?)

In *FQH* (in one direction) initial alignment (complete order) of nematic spins at the lowest temperature followed by spin relaxation. However, for each higher temperature, the numerical procedure takes the last (relaxed) spin configuration of the previous (a little lower) temperature before relaxation at this temperature begins.

In *AH,* the system involves gradually decreasing the temperature from the isotropic phase. At each temperature, we equilibrate a structure and use its configuration for the starting profile at the next slightly lower temperature. We denote this history as an *AH*.

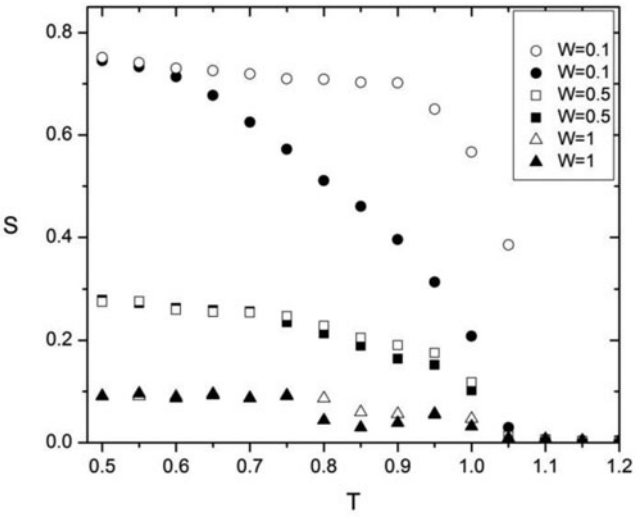

Figure 1. Hysteresis behavior *S(T)* in different values of anchoring strength *W*. "Up" (empty symbols) corresponds to increasing *T* "Down" (full symbols) corresponds to decreasing *T*, $p = 0.1$, N = 70.

Hysteresis

In this section, we estimated phase behavior for different anchoring strengths *W*. We compare the degree of nematic order in systems which are first annealed in the absence of an external field from a high temperature ($T = 1.2$) down to zero temperature (this is the AH discussed above), and then slowly heated back to the initial temperature. At each stage, the temperature is reduced or increased by *0.02* in scaled previous temperature. The system allowed then to relax to a steady state.

In Fig. 1 the *S(T)* dependence is shown for different anchoring $W = 0.5$,$W = 1$ and $W = 2$. It could be seen that by increasing anchoring strength *W* the degree of orientational ordering decreases.

Field Quenched History (FQH)

Next we consider *FQH*, it initiates the simulations from LC structures homogenously aligned a single symmetry breaking direction.

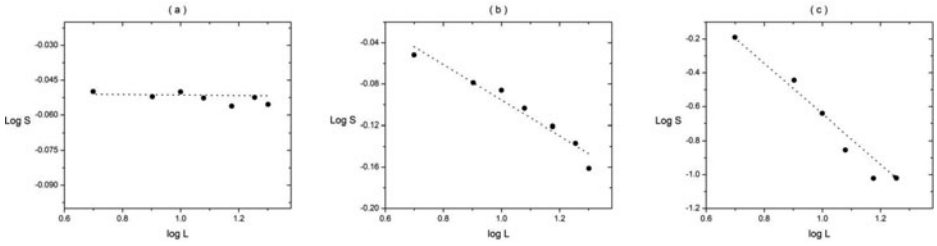

Figure 2. Finite size analysis of structures in *FQH*. Dashed curves are the fits using Eq.(10). (a) **LRO**: $W = 0.01$, $p = 0.1 \rightarrow \gamma = 0.0$ (b) **QLRO**: $W = 1$, $p = 0.1 \rightarrow \gamma = 0.17 \pm 0.17$ (c) **SRO**: $W = 2$, $p = 0.3 \rightarrow \gamma = 1.54 \pm 0.13$ All simulations performed at $T = 0.5$, $N = 70$.

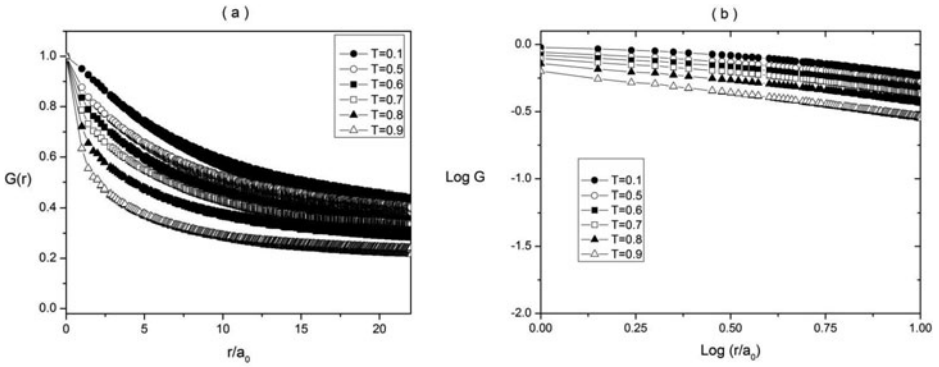

Figure 3. (a) *G(r)* Plot (b) Corresponding Log-Log plot for *FQH* in different T, $W = 1$, $p = 0.1$, $N = 70$.

The present study determines the exact character of the phase transitions for a given choice of coupling parameters. To investigate this problem, the finite size analysis done, this has shown in Fig. 2. In this figure, we plotted different ordering structures for showing that how much anchoring strength W and concentration p, influence on range of order. By comparison between Fig. 2(a) and Fig. 2(b) we can conclude that by increasing W, *QLRO* can be appeared and in high values of W and p the *SRO* established (Fig. 2(c)). In next sections we compared divergent histories (*FQH, TQH* and *AH*) in different impurity concentration p and temperatures T that showed in Figures 7, 8 and 9.

In Fig. 3a and Fig. 3b we have shown the correlation function *G(r)* defined via Eq.(8) for different temperatures in the *FQH* and also Log –Log plot. It exhibits *QLRO* the correlation function for all temperatures and it has a good superimposible fit with according to Eq. (9c) for the components in the low T and by increasing temperatures it is inclined to *SRO*.

In Figs. 4 and Fig. 5, we present representative $G(r)$ profiles at $T = 0.1$ for different values of p. The analysis indicates that for very weak coupling p, the system for *FQH* is exhibiting *QLRO*, Moreover, the concave form of the log-log plots strongly approved with decreasing the range of the order as the degree of p increases.

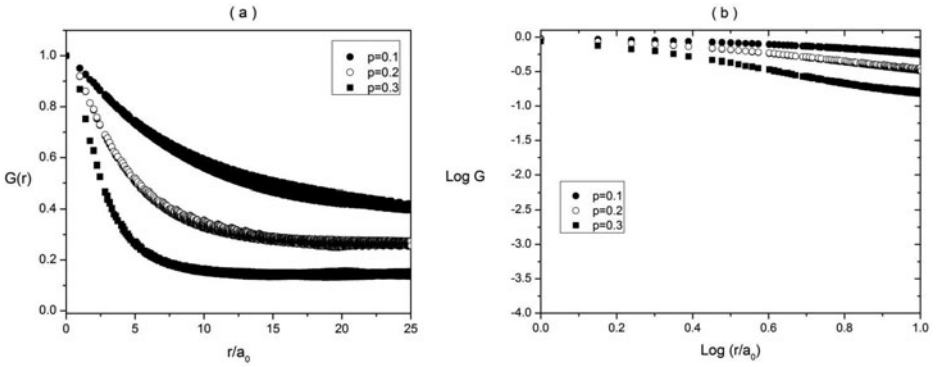

Figure 4. Variation of *G(r)* as a function of impurity concentrations p for *FQH*, at constant impurity strength $W = 1$, $(T = 0.1, L = 70)$. (a) *G(r)* plots; (b) log-log plots.

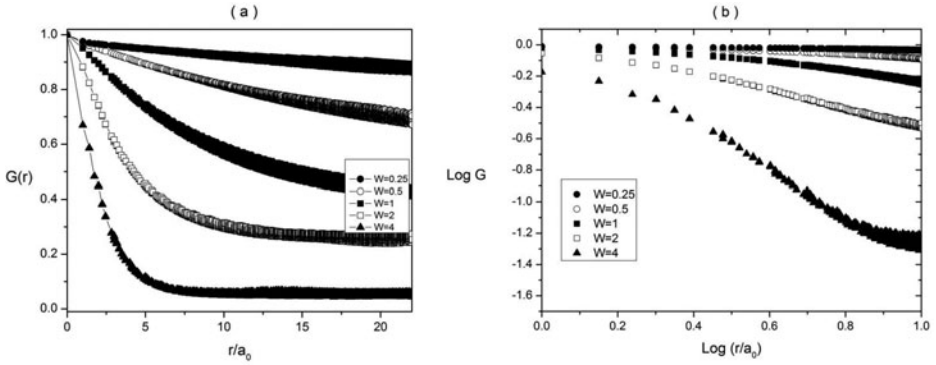

Figure 5. Variation of $G(r)$ as a function of impurity strength W for FQH, at constant impurity concentration $p = 0.1$ ($T = 0.1$, $N = 70$). (a) G(r) plots; (b) log-log plots.

In Fig. 5 we showed $G(r)$ profiles at $T = 0.1$ and $p = 0.1$ for different values of W in FQH. For low coupling anchoring W (i.e. $W = 0.25$) we can see LRO and for $W = 0.5$ and $W = 1$ are $QLRO$ apparently, but for higher value of W, the SRO can be established, the concave form of the log-log plot strongly proves that.

The dependence of correlation length ξ on temperature T, in different anchoring W and concentration p are really interesting. The size of domain ξ is estimated by using anstaz of equation (9a) where $\xi \sim 1/k$ and it shows in Fig. 6a and Fig. 6b.

They are evident from Figs. 6a and 6b that by increasing anchoring W and concentration impurities p the size of domain declined. The high interactions and elastic forces between LCs and impurities that tend to establish a homogeneous structure are the main reason. The observed SRO is the Imry-Ma theorem [34] that claiming even very weak random filed type disorder can destroy the LRO of a pure system reached via a continuous symmetry-breaking transition.

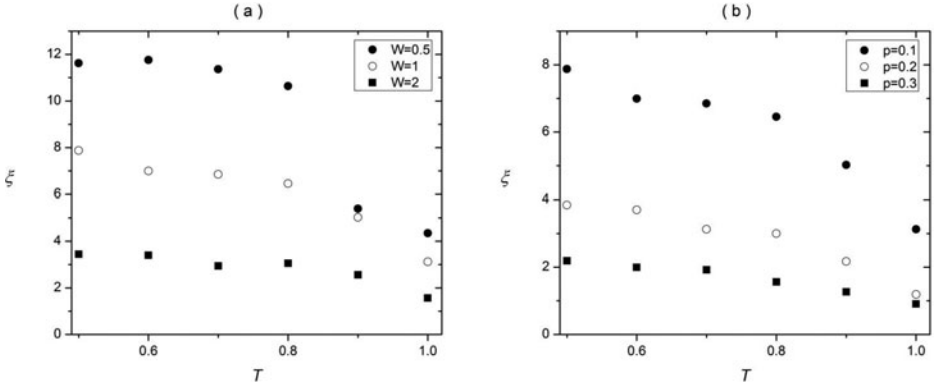

Figure 6. Dependence of correlation length ξ as a function of T in FQH (a) Different W $p = 0.1$, $N = 70$ (b) Different p, $W = 1$, $N = 70$.

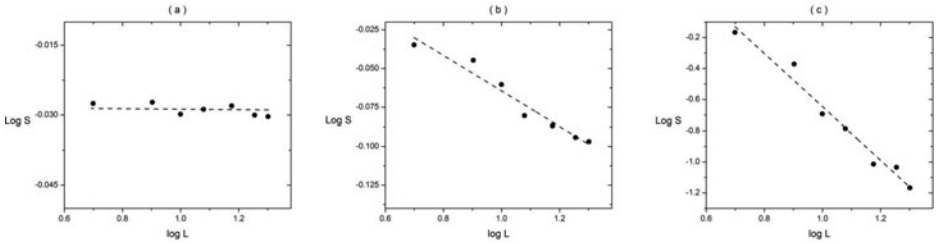

Figure 7. Finite size analysis of structures in *TQH*. Dashed curves are the fits using Eq.(10). (a) ***LRO***: $W = 0.01$, $p = 0.01 \rightarrow \gamma = 0.0$ (b) ***QLRO***: $W = 1$, $p = 0.1 \rightarrow \gamma = 0.114 \pm 0.11$ (c) ***SRO***: $W = 2$, $p = 0.3 \rightarrow \gamma = 1.61 \pm 0.12$ All simulations performed at $T = 0.5$, $N = 70$.

Temperature Quenched History (TQH)

We now turn definitely to Temperature quenched history (*TQH*). For showing different range of ordering in *TQH,* we analyzed the finite size structures in different W that has shown in Fig. 7. In this figure, it shows that how much anchoring strength W and concentration p affects to range of order. By comparison between Figs. 7 we can conclude that by increasing W, *QLRO* and by increasing W and *p, SRO* can formed.

In Figs. 8, 9 and 10 we plotted a typical *G(r)* profile for *TQH* for different values of p, W and T. From Fig. 8, it seems that for given value concentration *p,* the *SRO* is established appropriately. The other ranges could not establish at all.

Nevertheless, in Fig. 9 for very weak coupling W, the *QLRO* might formed, because log-log plot shows very slightly decline, moreover, the analysis indicates that for high value of *W,* the systems are exhibiting *SRO*, and the curve form of the log-log plot strongly proved that. As a Consequent, the crossover between regimes is difficult to define precisely.

In Fig. 10 we plotted a typical *G(r)* profile for *TQH* at $p = 0.1$and $W = 1$ for various values of T. It can be seen that in all temperatures range order is quite *SRO*. This is really differing from Fig. 3 that we saw *QLRO,* for given temperatures T for *FQH*.

The size of domain ξ for *TQH* in different W and p has studied. As we expected with increasing both values the size of domain ξ declined. That shows with increasing T the

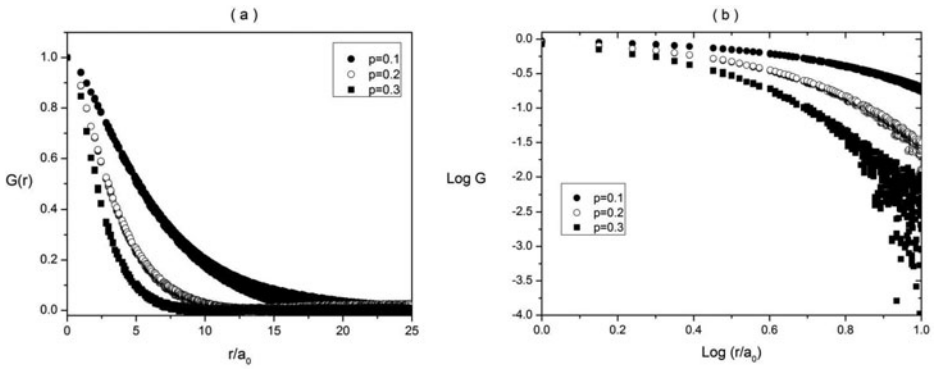

Figure 8. Variation of *G(r)* as a function of impurity concentrations p for *TQH*, at constant impurity strength $W = 1$, $T = 0.1$, $L = 70$. (a) G(r) plots; (b) log-log plots.

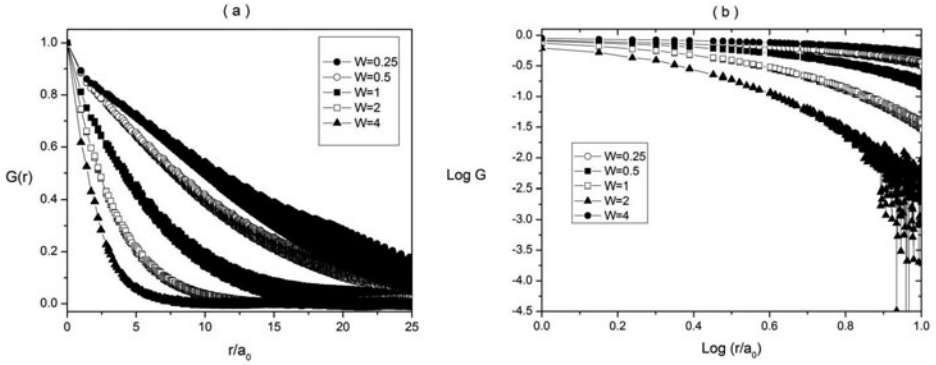

Figure 9. Variation of $G(r)$ as a function of impurity strength W for TQH, (a) natural plots; (b) log-log plots. $T = 0.5$, $p = 0.1$, $N = 70$.

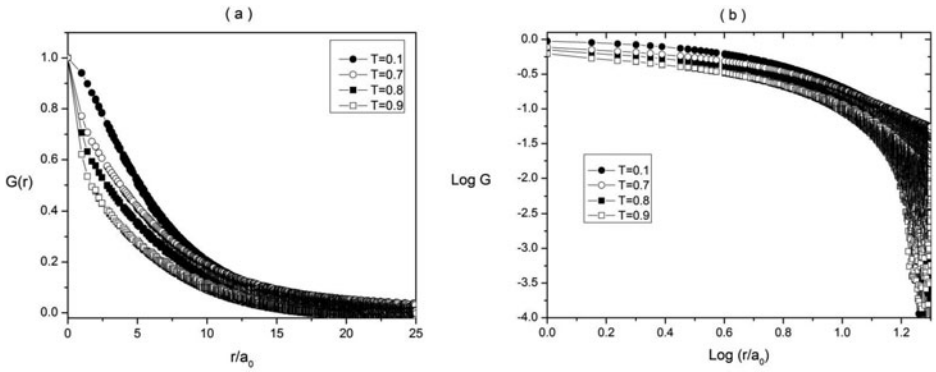

Figure 10. (a) $G(r)$ Plot (b) Corresponding Log-Log plot for TQH at different T, $W = 1$, $p = 0.1$, $N = 70$.

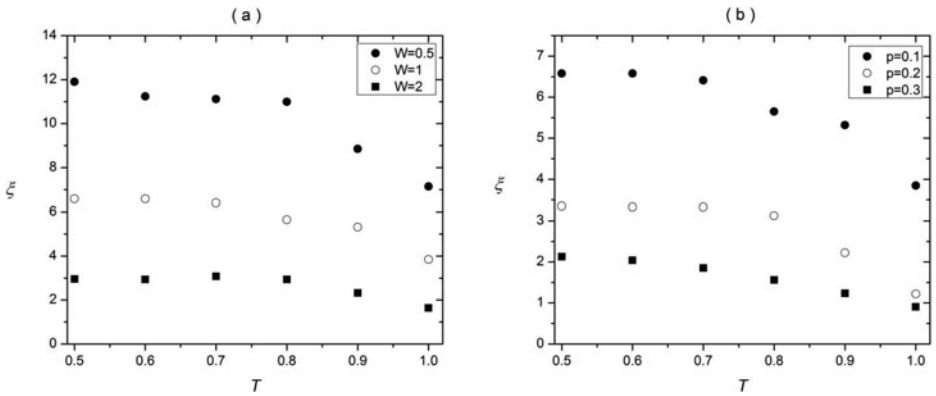

Figure 11. Dependence of correlation length ξ as a function of T in TQH (a) Different W, $p = 0.1$, $N = 70$ (a) Different p, $W = 1$, $N = 70$.

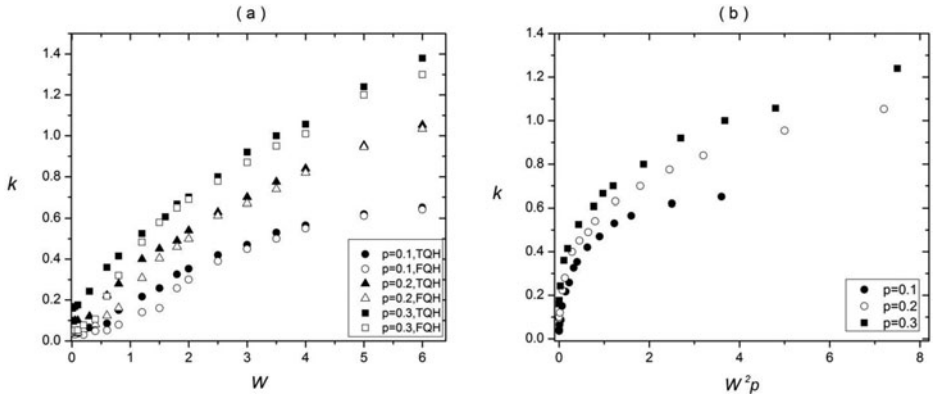

Figure 12. Dependence of the size $k = \xi^{-1}$ of Imry-Ma domains, obtained by fitting simulation *G(r)* to the exponentially decaying form given by eq.(9c), (a) $\xi(W)$ for different values of p in two different histories;Only is for *TQH*. In both plots, $T = 0.1$, $N = 70$.

formation of domains are going to be shrink due to decreasing of elastic forces for spatial homogenous pattern. The results have shown in Figs. 11a and 11b.

Comparison of Histories

In this section, we compared variety of histories in different *p, T* and three different histories *TQH, FQH* and *AH*.

In Fig. 12 we plotted $k(1/\xi)$ as a function of W at $T = 0.1$ at different values of p. In the high values of anchoring strength, the values of ξ saturated, in contrary, in the weak interaction region $W<1$ the Imry-ma scaling is realized. From this figure could be concluded that by exceeding concentration p, the correlation length ξ reduced. The reason behind this behavior is increasing interactions between LCs and impurities. In the weak coupling regime it has a good agreement with the predictions of Imry-ma scale $\xi_d \propto W^{-2}$[4]. We

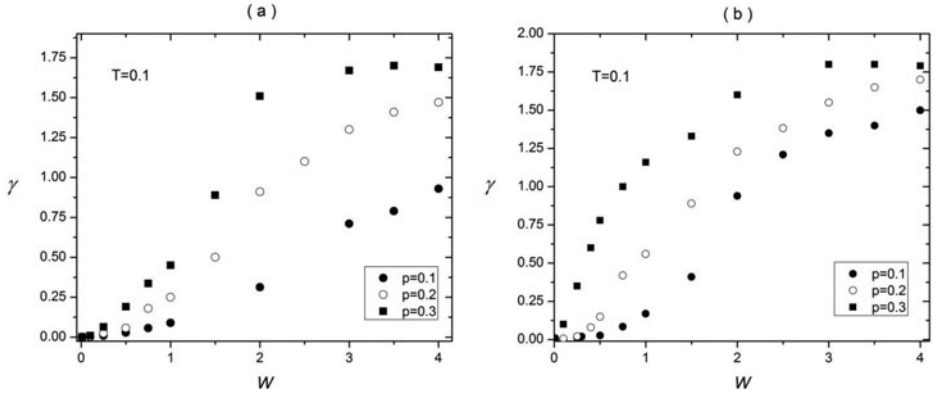

Figure 13. Value of γ obtained from the finite size analysis using Eq.(10). *LRO* and *SRO* are signaled by $\gamma = 0$ and $\gamma > 1.5$ respectively. In the regime $0 < \gamma < 1.5$ *QLRO* is expected. (a)The *FQH* (b) *TQH*, $T = 0.1$, $N = 70$.

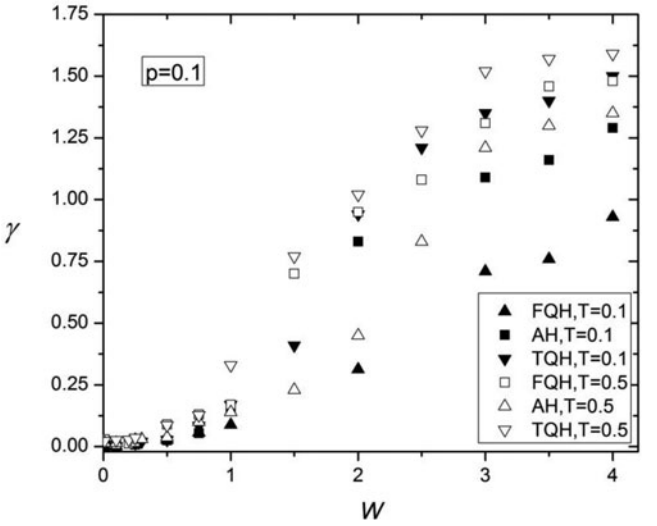

Figure 14. Comparison of phase structures derived by *FQH* (triangle), *AH* (Square) and *TQH* (reversed triangle) for $T = 0.1$ (full symbols) and $T = 0.5$(Empty symbols), $p = 0.1$, $N = 70$.

expect that domain sizes will not be smaller than the distance between impurities, and therefore universality would be lost for higher pW^2.

In Figs. 13a and 13b we plotted γ as a function of W for different values of p in two regimes *FQH* and *TQH* individually. In the *FQH* one sees that *SRO* is realized in for strong enough values of W *(i.e.* $W \geq 2$) and high concentration impurities p (i.e. $p = 0.3$). However, in *TQH* has also seen *SRO* in $p = 0.2$ in high value of W. Note that in very weak

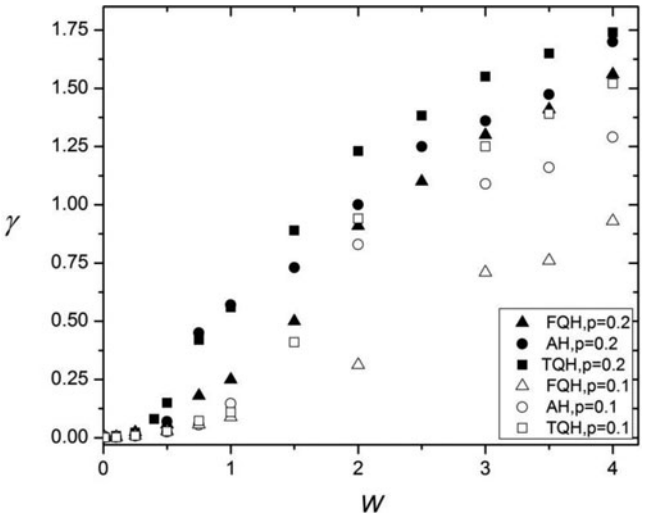

Figure 15. Comparison of phase structures derived by *FQH*, *AH* and *TQH* at two different p. $T = 0.1$, $N = 70$.

coupling regime *LRO* might realized. Our simulations suggest that for $p = 0.1$, *LRO* exited for $W << 0.1$ for *FQH* also for $p << 0.1$ and $W << 0.1$ for *TQH* [Figs. 2, 7].

In Fig. 14 presents the nature of order indicated by value of gained from finite size scaling using Eq.(10). The *LRO* is signed by $\gamma = 0.0$ limited to very low W in both cases *TQH* and *FQH*. The *QLRO* occurs in $0 < \gamma < 1.5$ for intermediate *W,* for *TQH* and *FQH*. But, The *SRO* occurs just at *TQH* in higher value of W and T (i.e.,$W \geq 3$, $T = 0.5$). We have not seen any *SRO* for other cases at $T = 0.1$. The Structural characteristics for *AH* are between those obtained for *FQH* and *TQH*.

For more comparison about phase structures between three different histories, we plotted Fig. 15 in the two different concentration of impurities *p.* It can be founded out that at $p = 0.2$ with increasing value of $W \geq 3$, *SRO* established for *TQH*, and $W = 4$ for *AH*, but we have not seen for *FQH*. At $p = 0.1$ we saw *SRO* in very low anchoring strength W and *QLRO* for other calculated *W.* It could not create *LRO* for this concentration.

IV. Conclusions

We have studied a model of liquid crystals embedded in porous media. The model uses rod-like objects with $D_{\infty h}$ symmetry within a cubic lattice interacting via a Lebwohl–Lasher-type interaction. The system contains impurities at concentration p, which impose a random anisotropy field. We analyzed the domain-type pattern of molecules as a function of p, and *W,* where W is the anchoring strength between a neighboring director and impurity. This model is a generalized amalgam of the RAN [10] and SSS [8] models.

The study has concentrated on the effect of sample history on the observed phase behavior. We have distinguished three separate histories, which we have labeled *TQH*, *FQH* and *AH*. In *TQH* we quench a randomly orientationally distributed nematic spin configurations to a low temperature $T << T^*$, and then allow the system to equilibrate. In *FQH*, by contrast, we let a set of aligned nematic spins to relax. The *FQH* assumed sufficiently large for the nematic spins initially completely aligned. Finally, in *AH* we examined annealed samples, in which the temperature was slowly decreased from a high temperature sample in which there was no initial nematic ordering.

We have distinguished three separate phase regimes, identified with Imry-Ma clusters (short-range order SRO), algebraic or quasi-long-range order (QLRO) and true long-range order (LRO). We have studied increasing anchoring strength *W,* for both regimes *TQH* and *FQH*. In *FQH*, all three regimes appeared. The *LRO* exist in low value of W, *QLRO* and *SRO* in high value can appear. However, in *TQH*, just *SRO* formed.

When comparing two different histories at the same temperature T, we found that in *FQH* for given temperatures T (from $T = 0.1$ *to* $T = 0.9$), only *QLRO* occurs. A Log-Log plot of the mean order parameter for the sample confirms this finding. In addition, our study examined different concentrations of impurities p. In the FQH, at high values of p we found *SRO*, whereas at low values of p, we always found *QLRO*. By contrast, for *TQH,* we saw only *SRO*.

The study also used finite-size scaling methods in one constant temperature *($T = 0.5$)* to distinguish phases in *LRO*, *QLRO* and *SRO*. In our studies of systems subject to *FQH,* we find results consistent with *LRO* for very low anchoring strength *W (i.e.* $W = 0.1$*)* and very low concentration impurities *p (i.e.* $p = 0.01$*)*. It is possible, however, that these are simply system size effects. As W and p are increased, first *QLRO* and then *SRO* phases form. However, the crossover between these regimes is sometimes difficult to determine exactly. As a result, we have only been able to estimate crossover values of W approximately. Finally, for *TQH, LRO* occurs at very low anchoring strength *W (i.e.* $W = 0.01$*)* and low

concentration impurities *p (i.e. p = 0.01)* (although again this may be a small-system-size effect). For higher values of *W* and *p*, *QLRO* and *SRO* were observed.

A related study also analyzes simulation results as a function of *W*, for a number of different concentrations *p*, for two separate temperatures *T (T = 0.1* and *T = 0.5)* in all regimes *TQH, FQH* and *AH,* and obtained an approximate phase diagram as a function of *W*, for different fixed values of *p*. In general, in the weak coupling regime Imry-Ma scaling $\xi_d \propto W^{\frac{-2}{(4-d)}}$ is approximately obeyed. A general conclusion of our work is that initial conditions and history can significantly influence the observed phase behavior of these models, and by extension of liquid crystals in pores.

Acknowledgments

This work was started when T.J. Sluckin visiting professor in the Faculty of Physics, University of Maribor. He thanks the Ministry of Education, Government of Slovenia for their generous grant over the period October-December 2011, and is grateful to Professor N. Vaupotič (Dean of the Faculty) for her hospitality over this period. S. Kralj and T.J. Sluckin acknowledge the hospitality of the Isaac Newton Institute for Mathematical Sciences, Cambridge, UK, where both were programme visitors in the 2013 "Mathematics of Liquid Crystals" programme, and where much of this work was completed. We also thank R. Pelcovits (Brown), C. Zannoni (Bologna) and particularly P. Shukla (NEHU, Shillong, India), for helpful discussions. S. Kralj acknowledges the support of the European Office of Aerospace Research and Development Grant FA8655-12-1-2068. A. Ranjkesh acknowledges the support of a Slovenian Research Agency (ARRS) young researcher grant.

References

[1] Feldman, D. E, (2001). *Int. J. Mod. Phys. B*, *15*, 2945.
[2] Feldman, D. E. & Pelcovits, R. A, (2004) *Phys. Rev. E*, *70*, 040702.
[3] Iannacchione, G. S. (2004), *Fluid Phase Equilibria*, *222–223*, 177–187.
[4] Harris, R., Plischke, M. J., & Zuckermann, M. J, (1973) *Phys.Rev. Lett. 31*, 160.
[5] Feldman, D. E., (2000). *Phys. Rev. Lett.*, *84*, 4886.
[6] Crawford, G. P. & Žumer, S.,(1996). *Liquid Crystals in Complex Geometries Formed by Polymer and Porous Network*, Oxford University Press: London, UK.
[7] De Gennes, P. G., & Prost, J.,(1993). *The Physics of Liquid Crystals*, Oxford University Press: Oxford, UK.
[8] Bellini, T., Buscaglia, M., & Chiccoli, C. (2000). *Phys. Rev. Lett.*, *85*(5), 1008–1011.
[9] Bellini, T., Radzihovsky, L., Toner, J. & Clark, N. A. (2001). *Science*,*294*, 1074.
[10] Cleaver, D. J., Kralj, S., Sluckin, T. J. & Allen, M. P.,(1996). *The random anisotropy nematic spin model, in Liquid crystals in complex geometries formed by polymer and porous networks*, edited by Crawford, G. P. & Zume, S., *Taylor and Francis, Chap. 21*.
[11] Radzihovsky, L. & Toner, J. (1997). *Phys. Rev. Lett.*, *79*, 4214.
[12] Ranjkesh, A., Ambrozic, M., Cordoyiannis, G., Kutnjak, Z. & Kralj, S. (2013). *Advances in Condensed Matter Physics*, *2013*, 505219.
[13] Repnik, R, Ranjkesh, A, Simonka, V, Ambrozic, M, Bradac, Z, & Kralj, S. (2013). *J. Phys: Condens. Matter*, *25*, 404201.
[14] Bellini, T., Clark, N. A., Muzny, C. D., Wu, L., Garland, C. W., Schaefer, D. W., & Oliver, B.,(1992). *Phys. Rev. Lett*, *69*, 788–791.
[15] Kralj, S., Zidanšek, A., Lahajnar, G., Muševič, I., Žumer, S., Blinc, R., & Pintar, M. M. (1996). *Phys. Rev. E*, *53*, 3629–3638.
[16] Kutnjak, Z., Kralj, S., Lahajnar, G., & Žumer, S. (2002). *Phys. Rev. E*, *66*. 041702.
[17] Popa-Nita, V. (1999). *Eur. Phys. J.*, *83*, 12.

[18] Tripathi, S., Rosenblatt, C., & Aliev, F. M.,(1994). *Phys. Rev. Lett. 72*, 2725–2729.
[19] Chakrabarti, J.,(1998). *Phys. Rev. Lett. 81*, 385.
[20] Kralj, S., Zidanšek, A., Lahajnar, G., Muševič, I., Žumer, S., Blinc, R., & Pintar, M. M. (1996). *Phys. Rev. E*, *53*, 3629–3638.
[21] Kutnjak, Z., Kralj, S., Lahajnar, G., & Žumer, S. (2003). *Phys. Rev. E*, *68*, 021705.
[22] Sinha, G., Leys, J., Glorieux, C., Thoen, J. (2005). *Phys. Rev. E*, *72*.
[23] Buscaglia, M., Bellini, T., Chiccoli, C., Mantegazza, F., Pasini, P., Rotunno, M., & Zannoni, C. (2006). *Phys. Rev. E.*, *74*, 011706.
[24] Ranjkesh, A., Ambrožič, M., Kralj, S., & Sluckin, T. J. (2014). *Phys. Rev. E*, *89*, 022504.
[25] Iannacchione, G. S., Garland, C. W., Mang, J. T., & Rieker, T. P. (1998) .*Phys. Rev. E*, *58*, 5966–5981.
[26] Fabbri, U. & Zannoni, C. (1986). *Mol. Phys. 58*, 763.
[27] Popa-Nita, V. (1999). *Chem. Phys. 246*, 247–253.
[28] Popa-Nita, V. & Romano, S. (2001). *Chem. Phys.*, *91*, 264.
[29] Kralj, S, Bradac, Z, & Popa-Nita, V. (2008). *J. Phys.: Condens. Matter*, *20*, 244112.
[30] Virga, E.G., (1994). *Variational Theories for Liquid Crystals*, Chapman Hall: London, Uk.
[31] Ambrožic, M., Kralj, S., & Virga, E.G. (2007). *Phys. Rev. E*, *75*, 031708.
[32] Bellini, T., Buscaglia, M., Chiccoli, C., Mantegazza, F., Pasini, P., & Zannoni, C., (2002). *Phys. Rev. Lett. 88*, 245506.
[33] Lebwohl, P. A. & Lasher, G. (1972). *Phys. Rev. A*, *6*, 426.
[34] Imry, Y. & Ma, S. (1975). *Phys. Rev. Lett*, *35*, 1399.
[35] Eppenga, R. & Frenkel, D. (1984). *Mol. Phys*. *52*, 1303.
[36] Binder, K. & Heermann, D. W., (1988), *Monte Carlo Simulation in Statistical Physics; An Introduction*, Springer, Chap. 2.3.
[37] Feldman, D. E., (2001), *Int. J. Mod. Phys, B*, *15*, 2945.